Journal of INTELLIGENT CONSTRUCTION

Research Article/Review
https://doi.org/ 10.26599/JIC.2025.9180076

Effect of microstructure differences on the thermal and mechanical behaviors of porous cementitious composites using phase change materials

Md Suman Mia[a,*,(✉)], Satya Medepalli[a], Yuya Takahashi[a,(✉)], Koichi Tsuchiya[b], Tetsuya Ishida[a]

[a] *Department of Civil Engineering, The University of Tokyo, Japan*
[b] *Research Center for Structural Materials, National Institute for Materials Science, Japan*
** Department of Civil Engineering, Dhaka University of Engineering & Technology, Gazipur, Bangladesh*

Received: 2024-05-08 ***Revised:*** 2024-07-02 ***Accepted:*** 2024-07-10

ARTICLE INFO

Keywords
PoroPCM
Heat storage capacity
Functional building material
Sustainable building practices

ABSTRACT

This study focuses on the effect of different microstructures on the thermal and mechanical behaviors of porous concrete impregnated with phase change materials (PCM), referred to as PoroPCM. This study involved the preparation of a PCM embedded cement paste, which included a 20% volume replacement of paraffin-based melamine–formaldehyde-coated microencapsulated PCM. The prepared PCM embedded cement paste was mixed with approximately 20%, 40%, and 60% volume substitutions of the aerated foam to prepare the PoroPCM specimens. Two series of specimens were prepared by using two distinct mixing methods. One involved gentle mixing at a low energy, whereas the other used a high-speed mixer. X-ray computed tomography (CT) was used to visualize the 3D microstructures of the PoroPCM specimens. The datasets extracted from the X-ray CT scans were reconstructed to quantify the spatial distribution of the pore network and analyze their effects on the thermal and mechanical behaviors, which were used to understand the governing parameters with different pore networks. The thermal behavior was measured in a temperature-controlled environmental chamber by placing a thermocouple at the center of the 100 mm cube specimens. The results indicated a significant enhancement in the thermal performance (delay in temperature increase) of the PoroPCM specimens owing to the phase transition and heat storage capacity of the PCM particles. In addition, the thermal behavior appeared to be influenced by the porosity, size distribution of the air voids, and internal moisture content, which were due to changes in the microstructure of the PoroPCM. Compressive strength tests revealed that the failure behavior of PoroPCM under a compressive load was ductile with a large deformation, and the failure was propagated by the disaggregation of a local collapse of the pore walls. Compressive strength is influenced by porosity; however, the influence of pore size is limited.

1 Introduction

Thermal energy storage using cementitious materials has gained significant attention in recent years because of the need to reduce energy consumption for heating and cooling in buildings. Phase change material (PCM) embedded cementitious composites enable thermal energy storage through phase transitions and enhance the energy efficiency of buildings [1]. PCMs can absorb and release significant amounts of latent heat during heating and cooling, and have low thermal conductivity [2], which may reduce the thermal conductivity of cementitious composites. Since, porous foam concrete with a higher air content can significantly improve the thermal insulation properties of cementitious materials, the adaptation of PCM to porous concrete based on the optimization of thermal conductivity and density is an efficient way to enhance energy storage with cementitious materials. In this context, a study was conducted on the coupling of PCM with highly insulated porous foam concrete. Porous cementitious composites incorporating PCMs are called PoroPCM [3], [4]. In PoroPCM, the PCM is primarily responsible for heat storage, and its thermal insulation property may be enhanced by reducing the overall thermal conductivity,

✉ Address correspondence to Md Suman Mia, suman105@duet.ac.bd; Yuya Takahashi; takahashi@concrete.t.u-tokyo.ac.jp

Citation: Md Suman Mia, Satya Medepalli, Yuya Takahashi, et al. Effect of Microstructure Changes on the Thermal and Mechanical Behaviors of Porous Cementitious Composites using Phase Change Materials. J Intell Constr, 2024, 2, 9180076.

© The Author(s) 2024. The articles published in this open access journal are distributed under the terms of the Creative Commons Attribution 4.0 International License (http://creativecommons.org/licenses/by/4.0/), which permits use, distribution and reproduction in any medi- um, provided the original work is properly cited.

through the air inside the pores. This novel functional material can be applied on building surfaces to enhance energy efficiency by shifting the peak temperature during extreme weather conditions [1]. The mechanical and thermal properties of porous materials depend heavily on their microstructures, particularly their porous structures [5]. PoroPCM is a lightweight material; from a structural point of view, reducing its density represents a considerable benefit, and its thermally insulating behavior can reduce cooling or heating costs, thereby reducing environmental pollution by reducing the heavy consumption of fuels [6].

Researchers have reported that the advantages of foam concrete include weight reduction, fire resistance, and good thermal insulation properties [7]. The air voids introduced by the foams constitute approximately 10–90% of the volume of hardened porous concrete, and their size distribution may affect heat transfer phenomena. The distribution of air voids inside porous concrete may be affected during preparation and may alter its mechanical and thermal performance, as well as its acoustic and durability properties [8]. The dry density, porosity, and pore size distribution of foam concrete directly affect the thermal and mechanical properties of cement-based materials [9]. Zhang et. al. [10] characterized the pore structure of foam concrete and suggested that the thermal insulation performance could be improved by increasing the porosity through the incorporation of a high volume of foam [11]. Lian et al. [12] discovered that the strength of porous concrete was significantly affected by the porosity of its internal structure. Wei et al. [9] noted that the heat transfer mechanism in foamed concrete is predominantly conduction, whereas other mechanisms, such as convection and radiation, are considered negligible owing to their smaller pore diameters.

Many researchers have adopted scanning electron microscopy (SEM), mercury intrusion porosimetry (MIP), and X-ray computed tomography (X-ray CT) to investigate pore networks in foam concrete. Recent advancements in X-ray CT techniques for the microstructural characterization of cementitious materials have been adopted by researchers [13]–[15]. Nguyen [13] characterized the mechanical behavior of foam concrete using X-ray CT; the results exhibited a significant change in the mechanical behavior, and the interconnected pores influenced the failure mechanism. Labdev et al. [16] studied the structure of cement-based cellular concrete using X-ray CT and showed that the pore structure of cellular concrete is dominated by capillary pores with a diameter of up to 200 μm. Nambiar and Ramamurthy [17] investigated the characteristics of the air-void structure in foam concrete and revealed that a narrower air-void size distribution imparts higher strength. Batool [18] investigated the effect of the microstructure on the thermal conductivity and heat flow of foam concrete. X-ray micro-computed tomography (CT) was used to quantify and visualize the 3D microstructures of the samples. Their results revealed that the pore size increased as the density of foam concrete decreased. The numerical results showed that the heat flow decreased with increase in porosity. In another study, Batool [19] characterized the size distribution of air voids in cement-based foam and observed its influence on thermal conductivity, density, and internal moisture content. Research has shown that, with an increase in the median void diameter, the thermal conductivity decreases, and the air void size distribution does not significantly affect the thermal properties. Furthermore, it was reported that smaller pores have a substantial influence on the conductivity.

Studies on PCM-embedded cementitious composites have largely focused on the characteristics and performance of energy storage systems and their applications. Various studies [20]–[22] have clearly shown that PCM cement paste has a more effective thermal energy storage than traditional materials. A review [23] summarized several studies that investigated the use of PCM in building energy storage systems. These studies found that PCM-embedded cement paste can be used in combination with other energy storage technologies to improve the overall performance of building energy systems. PoroPCMs may be a suitable solution for the effective storage and release of heat during periods of low and high solar radiation. Thus, the performance of PoroPCM should be evaluated by investigating the behavior of foam concrete combined with the PCM.

Based on the available literature, there has been no specific research evaluating the effects of microstructural differences resulting from different foam volumes and mixing methods on the thermal and mechanical behaviors of PCM-embedded cementitious materials. This study was undertaken to investigate the variation in void structures due to mixing methods and different foam volumes, and to compare the effect of the size distributions of air voids on heat transfer and mechanical behaviors. Furthermore, the influence of the air-void size distribution parameters on strength and thermal performance was investigated. The merit of this research is to understand how PoroPCM behaves when there are differences in its microstructure and to provide information to correlate the microstructures with its thermal and mechanical behaviors.

2 Material and Methodology

Figure 1 shows a graphical outline of the specimen preparation process. First, a PCM-embedded cement paste was prepared using a cement paste mixer. Table 1 lists the materials used and the mix proportions of the PCM-embedded cement pastes. The PCM content and water–binder ratio were maintained at 20% by volume and 0.40 by weight, respectively. An optimal percentage of PCM was selected based on a previous study [3], and a fixed value was used as the objective of the study is to focus on the effect of differences in microstructure on the thermal and mechanical performance of PoroPCM. The raw materials used in this study were similar to those used in a previous study [21]. The materials used for preparing the paste were water, ordinary Portland cement (OPC), blast furnace slag (BFS), silica fume (SF), lime-based expansive additives (Denka CSA), hardening accelerator (Facet), superplasticizer (SP), and microencapsulated PCMs (MPCMs) with a melting and freezing temperature of 28 °C and 21.5 °C, respectively. The hardening accelerator helps prevent variations in microstructure properties caused by density differences in PCM and cement particles in porous foam concrete by quickly solidifying and stabilizing the porous microstructure.

The MPCMs were collected from Miki-riken Industrial Co., Ltd., Japan and the following information was provided: The specific heat capacity and latent heat of MPCMs are 4.75 J/(g.K) and 170 J/g, respectively. It is a paraffin-based (powder type) melamine–formaldehyde-coated (heat resistance ~ 180 °C) hydrophobic material and has a spherical shape PCM with a diameter of approximately 65μm.

To prevent potential leakage, the PCMs were microencapsulated, and the percentage ratio of paraffin to melamine–formaldehyde was 70:30. A hydrophobic PCM was selected for this study to prevent water absorption and maintain a stable microstructure during mixing and preparation of specimens. The hydrophilic nature of the MPCMs may cause shrinkage of the PoroPCM specimens before hardening, owing to the absorption of water from the cement paste and lamellae of the air bubbles. In addition, hydrophobic PCMs may have less effect on the fluidity of the PCM embedded cement paste, which could be preferable for the preparation of PoroPCM.

Because the PoroPCM has a large void ratio, different admixtures were used to increase the strength of the matrix. Hardening accelerators were used to stabilize the foam and cement matrices. The aerated foam was prepared using a high-pressure foaming machine with a dilute solution of water and a foaming agent. Then, the PCM-embedded cement paste and aerated foam were mixed at a designated volume ratio to prepare PoroPCM. Two methods were used to mix the cement paste and foam, and three different foam volume fractions were prepared, as listed in the specimen series in Table 2. Low-energy gentle hand mixing (Series 1) and high-speed mortar mixing (Series 2) were used to alter the pore structures of the specimens, as shown in Figure 2. In the gentle hand mixing procedure, mixing was performed for approximately 60 s at an approximate speed of 15–18 rpm. For the high-speed mixing method, a high-speed mixture machine with a mass of 2.5 kg and a rotating speed of 550 rpm was used. A low mixing energy is required at a low mixing speed to reduce the collapse of air bubbles during mixing. Due to the unavailability of a low-speed mixer, hand mixing was utilized to achieve a low mixing energy. Three different foam volumes (20 %, 40 %, and 60 %) were used to determine the effect of porosity on the thermal and mechanical properties.

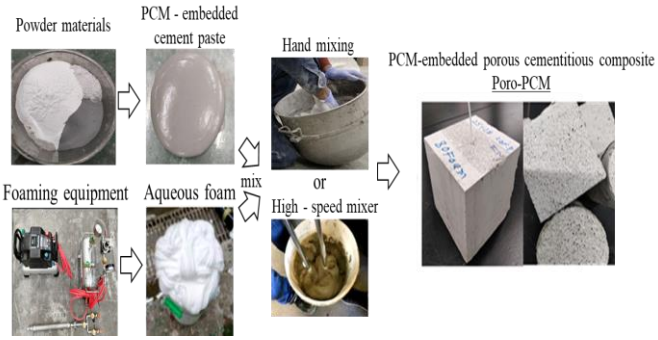

Fig. 1 PoroPCM preparation

(a) Gentle hand mixing method (b) High speed mixing method

Fig. 2 PoroPCM Mixing methods

Table 1 Materials and mix proportions of cement paste

Substance		Specific Density (kg/m³)	Unit volume of PCM-cement paste (kg/m³)
Water		1000	428
Binder	OPC	3150	535
	BFS	3100	449
	SF	2600	86
Facet		3000	22
Denka CSA		1080	11
SP		1070	13
MPCM		980	193

Table 2 Specimen series

Series	Mixing Method	Mixing ratio (Paste : Foam)
Series 1-20	Hand mixing	80:20
Series 1-40	Hand mixing	60:40
Series 1-60	Hand mixing	40:60
Series 2-20	High-speed mortar mixer	80:20
Series 2-40	High-speed mortar mixer	60:40
Series 2-60	High-speed mortar mixer	40:60

Cube specimens with dimensions of 100 mm × 100 mm × 100 mm and 50 mm × 50 mm × 50 mm and cylindrical specimens with dimensions of Ø50 mm × 100 mm were prepared for each specimen series to conduct thermal performance, X-ray CT, and compressive strength tests, respectively. After casting, all specimens were stored in an environmental room at which the controlled temperature is 20±2.0 °C and a relative humidity (RH) of 60±2%. After 28 d, the tests were conducted in the laboratory.

3 Experimental Investigation

3.1 *Weight measurement and void ratio*

The weight and size of each specimen were measured 28 d after casting. The void ratios of each series were measured based on the weight of a 100 mm cube specimen. Equation (1) was used to calculate the void ratio based on the weight of the specimens following the procedure described by Wei et al. [9], in which the voids of the foam concrete were also examined.

$$\emptyset = 1 - \frac{\rho}{\rho_t} \quad (1)$$

where $\emptyset$ is the void ratio, ρ is the weight of the specimen, and ρ_t is the weight of the solid PCM paste (without foam). Consequently, air bubbles derived from the aqueous foam were considered as voids.

3.2 *Microstructure Analysis*

X-ray CT was used to visualize the microstructures of the PoroPCM specimens. The main components of the CT scanner are an X-ray tube (radiation source), a rotating stage, and a flat panel detector. The inner view of the material was obtained by reconstructing the information received from the X-ray transmission while the sample holder and specimen were rotated 360°. The X-ray CT technique is based

on the absorption dependence of X-rays on material density and atomic number. Photons are emitted from the X-ray source toward the specimen, some of which penetrate the rotating sample and reach the detector, as illustrated in Figure 3 (a). When the X-rays pass through the specimen, the chemical components of the material absorb the intensity of the X-ray beam. Owing to the variation in X-ray attenuation within the specimen, the detected photons have a spectrum of energy and density, through which CT images with distinguishable contrast are generated. To organize the attenuation data captured at different angles, the general concept of back projection involves summating all the gathered projections across a two-dimensional space to recreate an image of the cross-section of the object, as illustrated in Figure 3 (b).

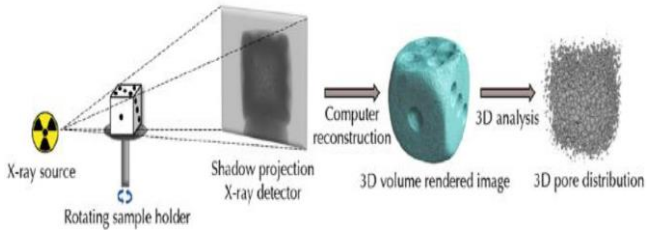

(a) Overview of the X-ray CT [24]

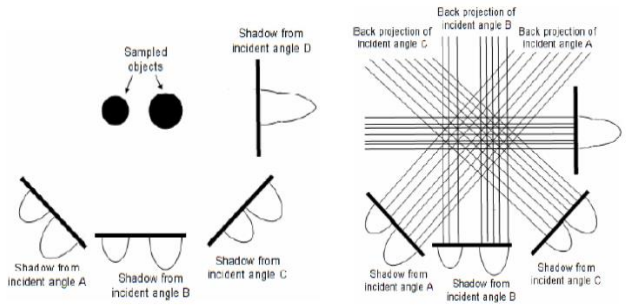

(b) X-ray attenuation at multiple incident angles [25].

Fig. 3 X-ray CT imaging principle and techniques

The size of the specimens used for the X-ray CT depended on the material and imaging parameters. For a higher resolution, the specimen must be placed near the source, and the sample size should be small. In this study, X-ray CT was performed on the porous specimens with 20%, 40%, and 60% foams. A small Ø10 mm cylinder was cut out of each 50 mm cube specimen, as shown in Figure 4, and a total of six specimens were examined using X-ray CT. The testing conditions were set as follows: X-ray source: 50 kV, 10 W, air filter, position of -45 mm, 4 x detector with a 30 mm projection, voxel size of 4.06 μm, and field of view (FOV) of 4.11 mm for Series 1 specimens; and air filter and position of -45 mm, 4 x detector with a 70 mm projection, voxel size of 2.66 μm, and FOV of 2.69 mm for Series 2 specimens. The stacked scan data from different imaging directions were saved on a computer as a matrix and reverted to pictures of different cross sections to reconstruct the 3D structure images of the material. The reconstructed CT images generally consisted of grayscale values of 8 or 16 bits, and the image size (number of pixels) was determined based on the CT resolution. Several post-processes, such as filtration and segmentation, have been performed to enhance the 3D structure of CT images. An image of the X-ray imaging process used for the investigating the microstructure is presented in Figure 4.

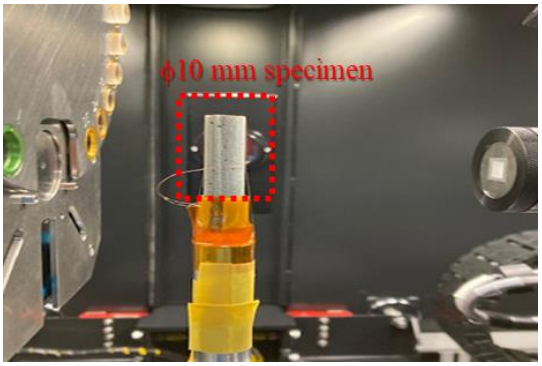

Fig. 4 X-ray imaging process of PoroPCM.

The pore network of the X-ray CT images was segmented using 8-bit grayscale images to produce binary images, as shown in Figure 5. The volume fraction of the segmented pores (porosity and pore size) was computed using the following algorithm, which comprises three main steps: The first step is the digitization of the X-ray CT images into mathematical matrices. Each voxel of the matrix represents the brightness of a pixel intensity, which varies from zero (black) to 255 (white). The second step in the reconstruction process is the segmentation of the paste and void phases using an appropriate color threshold. Owing to the high porosity and interconnected air voids, the threshold value is not well defined for the PoroPCM specimens. Threshold values for the segmentation of the binary images were selected based on the colors of the histograms of specimens 1-20 and 2-20, as shown in Figure 6, and applied to all specimens of the respective series. Threshold values of 86 for Series 1 and 98 for Series 2 were applied because of the different voxel sizes and testing environments during X-ray CT. The threshold is very important for quantifying the porosity and pore structures. Finally, the pore-size distribution of each specimen was quantified using the local thickness method [26], where each voxel represents the radius of the largest overlapping sphere.

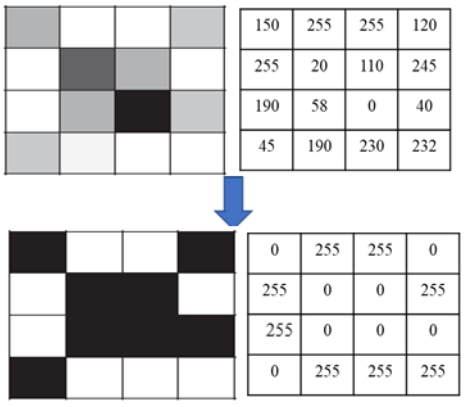

Fig. 5 Digitization of X-ray images by color threshold.

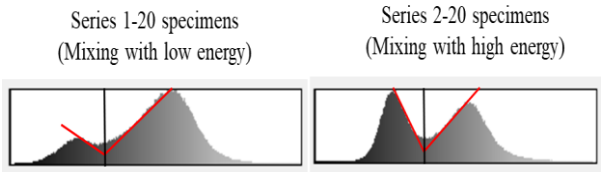

Fig. 6 Threshold setting of binary images.

3.3 Thermal Performance Test

The thermal performances of both series of PoroPCM specimens were evaluated using a temperature evolution test at 28 d and 35 d for Series 1 and Series 2, respectively. These difference in the test ages were due to the availability of an environmental chamber in the laboratory. Cube specimens with dimensions of 100 mm × 100 mm × 100 mm having thermocouples at the center were placed in a controlled environmental chamber with a programmed temperature variation of 15–35 °C for heating at a constant RH of 70%. Before testing, the specimens were kept in the environmental chamber at 15 °C for 48 h to keep the initial temperature similar to that of the environmental chamber. The environmental chamber and test specimens are shown in Figure 7. After completion of the test, the recorded temperature data were collected using the ThermoRecorder application of the thermocouples.

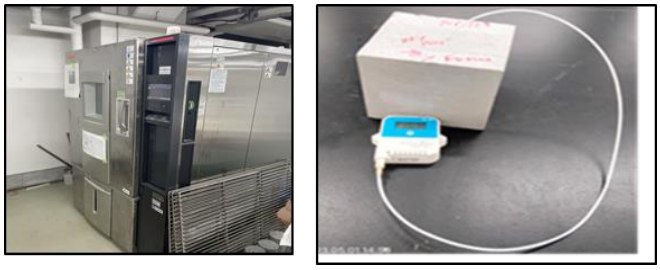

Fig. 7 Environmental chamber and test specimen for the thermal performance test

3.4 Mechanical performance

The compressive strength was measured to characterize the mechanical performance. Cylindrical specimens with dimensions of Ø50 mm × 100 mm were used. The loading rate was set at 0.5 mm/min until the specimens failed. Teflon sheets were placed at both ends of the specimens to reduce the friction between the loading plates and specimens during testing. The average values of the three specimens were used to calculate the compressive strength of each series.

4 Analysis and Results

4.1 Unit weight and void ratio

Figure 8 shows the measured unit weights of the specimens after 28 d. In the figure, the expected values from the mix proportions are presented as references. The unit weight of the specimens decreased with increasing foam volume. The results showed that the weight changes in the specimens for both series made using different mixing methods differed, even with the same amount of foam. The void ratios were calculated from the measured weights of the specimens using Equation (1), as shown in Figure 9. While Series 1-20 and Series 2-20 show a similar void ratio as displayed in Table 2, the other specimens in Series 1 show higher void ratios than Series 2–40 and Series 2–60 specimens. The variation in the void ratio is primarily attributed to the different mixing energies induced during the mixing of the PCM cement paste and foam. The Series 1 specimens were prepared by gentle hand mixing, and the required energy was relatively low, whereas the Series 2 specimens were prepared using a high-speed mortar mixer. Because of the high mixing energy, some large bubbles collapsed and altered the weight of the specimens by changing the internal foam volume of the freshly mixed PoroPCM, as shown in Figure 10. The addition of aqueous foam and PCM paste using different mixing methods create changes in the void ratio as well as in the amount of PCM content in the specimens. The Series 1–40 and 2–60 specimens occasionally showed similar void ratios in this study; therefore, they are compared in the following sections as specimens having the same void ratio but prepared using different mixing methods.

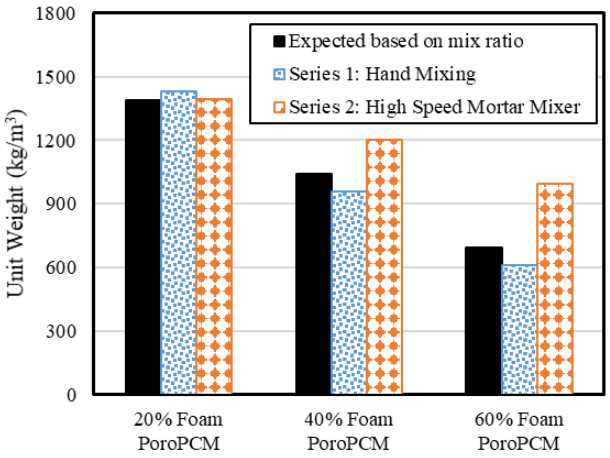

Fig. 8 Unit weight of specimens

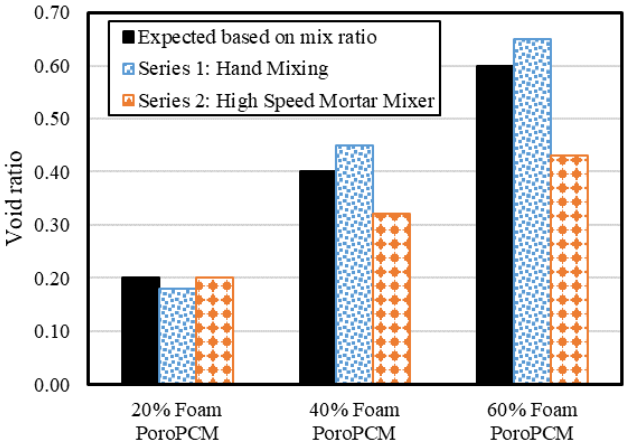

Fig. 9 Weight-based void ratio of specimens

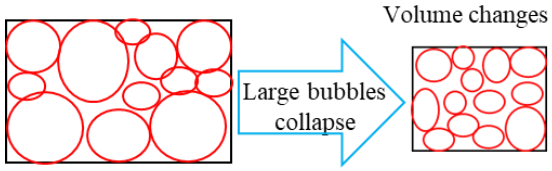

Fig. 10 Collapse of air bubbles during mixing.

4.2 Microstructure characterization of PoroPCM

X-ray CT measurements were conducted for both series of PoroPCM specimens, and microstructure characterizations were performed. The two series of grayscale images shown in Figure 11 were obtained with a voxel size of 4.06 μm for Series 1 and 2.66 μm for Series 2 and reconstructed for postprocessing using ImageJ and Python to quantify the porosity and pore network of the PoroPCM specimens. The PCM was well dispersed in the cementitious matrix. In addition, the porosity and PCM content were the same for the same mixing method and foam volume at different specimen heights, even if there was a difference in density. Figure 12 shows a comparison of the void size distributions obtained from the X-ray CT measurements of

Series 1 (gentle hand mixing) and Series 2 (high-speed mortar mixing) specimens. The variation in cumulative void ratios with air void diameter, for the specimens in the different series, is plotted in these figuresThe diameter of the voids was estimated as the equivalent diameter of a sphere with the same pore volume in the porous specimens. Although the void size distributions of the 20% foam specimens were similar regardless of the mixing method (Figures 12(a)), those of the 40% and 60% foam specimens differed according to the mixing method. In Series 1–40 and 1–60 specimens, relatively fewer voids smaller than 100 μm were observed, while voids larger than 300 μm were also present. For specimens with a higher foam content, the distance between the air bubbles was smaller, which increased the opportunity for the bubbles to merge into larger air bubbles (phenomena shown in Figure 13) after mixing. In Series 2-40 and 2-60 specimens, the number of voids smaller than 100 μm was the same as that of the 20% foam cases, and no voids larger than 300 μm were observed. This may be due to the collapse of the comparatively large air bubbles during mixing, as illustrated in Figure 8. As a result, the shape of the cumulative void-ratio curves differs with the mixing method for cases having higher foam content, which might affect the thermal and mechanical behaviors of the PoroPCM.

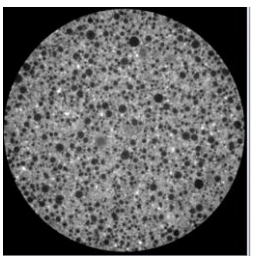

(a) Series 1-20

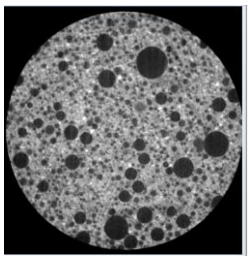

(b) Series 1-40

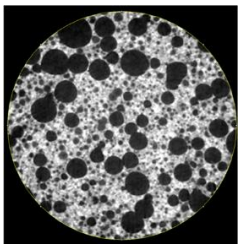

(c) Series 1-60

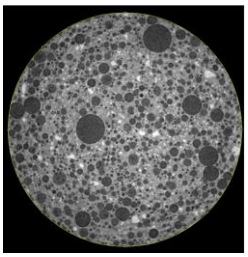

(d) Series 2-20

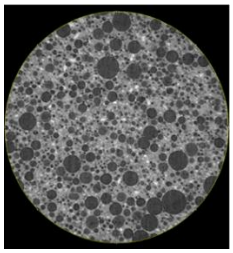

(e) Series 2-40

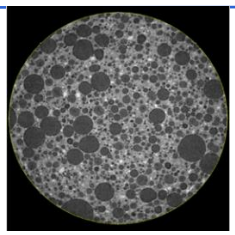

(f) Series 2-60

Fig. 11 Grayscale raw images of the microstructures of PoroPCM specimens.

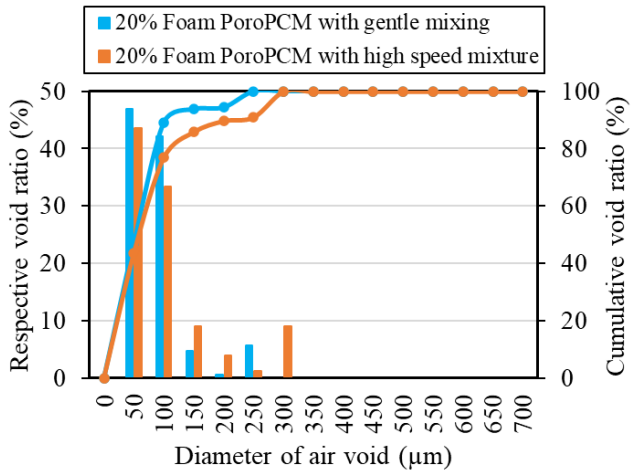

(a) Series 1-20 and 2-20 PoroPCM

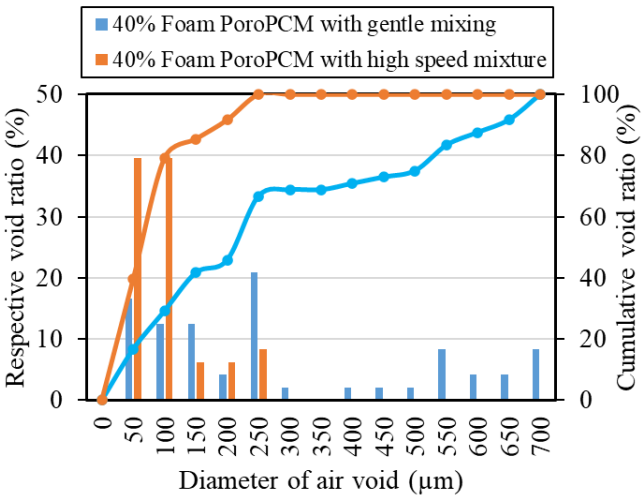

(b) Series 1-40 and 2-40 PoroPCM

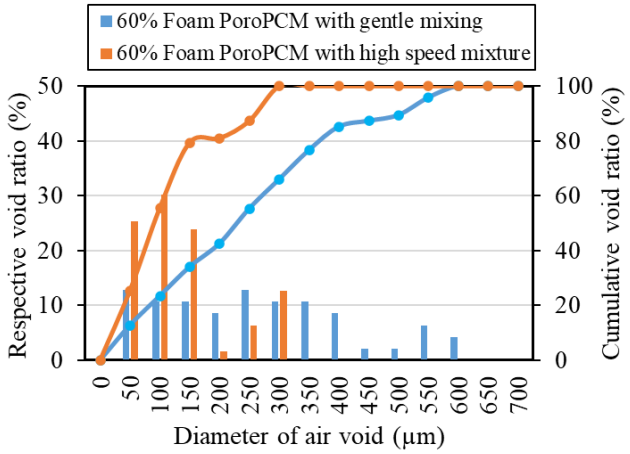

(c) Series 1-60 and 2-60 PoroPCM

Fig. 12 Void size distribution of PoroPCM specimens by X-ray CT

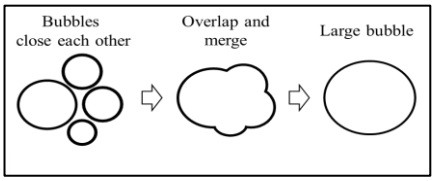

Fig. 13 Overlapping and merging of bubbles

Figure 14 shows the void ratios calculated using the reconstructed X-ray images of the specimens. The void ratios increased with the foam content; however, their tendency differed from that of the void ratios calculated from the weight measurements (Figure 9). The estimated void ratios were higher in Series 2 than in Series 1 even when the weights of the Series 2 specimens were higher (Figure 8). The reasons for these discrepancies are unclear; however, one possible reason is accumulated errors during the segmentation process. During the segmentation process, the 8-bit grayscale images were converted into binary images, which may have caused an overestimation of the fine-diameter void ratios. In addition, the resolution or voxel size of X-ray CT images may affect the accuracy of porosity estimation, because small voxel sizes are expected to be highly accurate because of the capture of more connected air voids. The voxel sizes of the X-ray images were found to be 4.06 and 2.66 μm for Series 1 and 2 specimens, respectively, which is why the estimation of the void ratio is more responsive for Series 2. However, the reason for this remains unclear, and further investigation is required. In this study, the void size distributions shown in Figure 12 are used in the following discussions as characteristics of void structures, whereas the void ratios were obtained from the weight measurements (Figure 8) and not from the X-ray CT results.

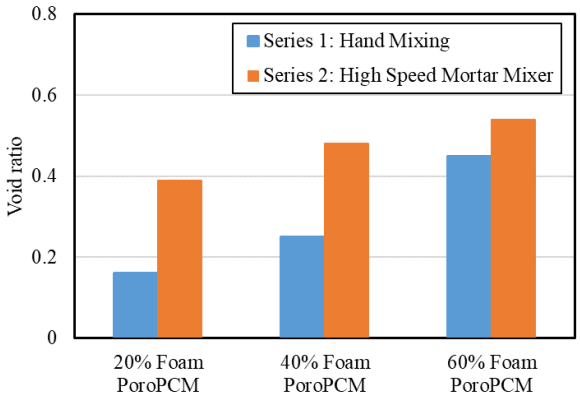

Fig. 14 Void ratios obtained from X-ray CT measurements

The median sizes (D_{50}) of the air voids from the void-size distributions are plotted against the void ratio calculated from the measured weights (Figure 8) in Figure 15. The median diameter of the voids increased with foam content for both series of specimens; however, the median void size was smaller in Series 2 than in Series 1. Here, the collapse of air bubbles during the mixing of paste and foam, and the overlapping and merging of air bubbles should be analyzed. As illustrated in Figure 8, the foam initially contains air voids of similar sizes before mixing; however, large voids collapse during the mixing of the paste and foam with high energy, resulting in differences in the weights of the specimens (Figure 8) and a narrower distribution of air voids in the case of Series 2 (high-speed mortar mixer) specimens compared to Series 1 (gentle hand mixing). Air voids of various sizes can exist in the case of a higher foam content at the beginning of mixing. They are very close to each other and can easily merge and form larger bubbles if they do not collapse during mixing. In addition, the mixing uniformity may influence void size distribution, and the mixing energy can cause different spatial distributions of micropore structure development in the specimens. A similar bubble formation process in cementitious composites was reported by Batool [19]. In Series 1 (hand mixing), the mixing energy was low and large bubbles remained after hardening. Consequently, the Series 1 specimens had a wide range of voids. Thus, the mixing method can affect the bubble merging and collapse processes, which manifest as different void ratios and void-size distributions. To maintain the void ratio at the desired foam content, a gentle mixing procedure is preferred, particularly at high void ratios.

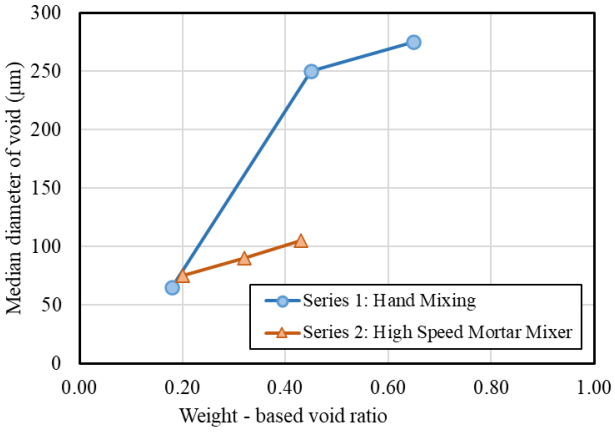

Fig. 15 Mean size of air voids with void ratio

4.3 Thermal performance

To evaluate the thermal performance, temperature tests were conducted in a controlled-environment chamber by placing a thermocouple at the center of the cube specimens. The ambient temperature was raised instantly from 15 to 35 °C while the RH was kept constant at 70%. The material ages of Series 1 and 2 specimens were 28 d and 35 d, respectively. Figure 16 shows the rise in internal temperature at the center of the 100 mm cube specimens during the temperature rise test. For all specimens, the temperature rise stagnated around the melting temperature of the MPCM owing to the absorption of latent heat by the MPCM. The temperature-rise delay (or temperature inflection point) behavior differed with different foam contents; specimens with higher foam contents had shorter temperature-rise delays. The specimens with a higher foam content had smaller amounts of MPCM per unit volume, which led to a smaller latent heat storage capacity, resulting in a shorter temperature inflection point. Therefore, the temperature delay period was shorter in cases with a higher foam content. In real-life situations, the peak temperature of a day is usually at midday and starts to decrease thereafter. The shift in the peak temperature time may be an indicator of a comfortable indoor temperature during drastic temperature transition conditions and may also reduce energy consumption, which is desirable for sustainable building practices. To control this temperature-rise delay period, the MPCM content in the PoroPCM material can be adjusted.

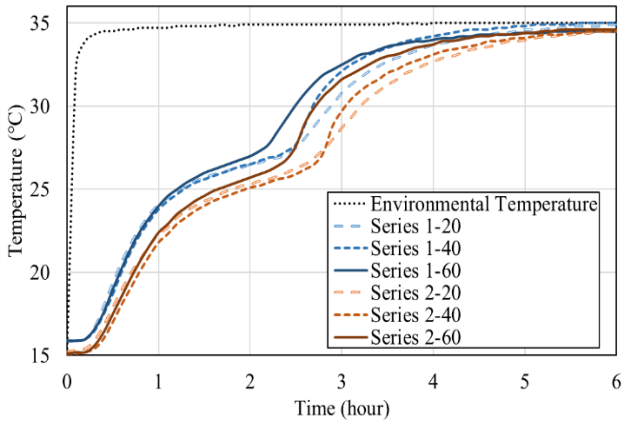

Fig. 16 Temperature test results of PoroPCM

Considering the initial temperature-rise period before MPCM melting, the rate of temperature increase appeared to differ for the different mixing methods. Series 2 specimens exhibited a slower increase in temperature than Series 1 specimens. Owing to the lower void ratio of Series 2 specimens (collapse of air bubbles during mixing with high energy), the variation in the amount of embedded PCM may alter the heat storage capacity. Even with the same void ratios (like Series 1–40 and 2–60), different heat transfer rates from the outside to the center of the specimen were observed. This can be caused by the different bulk thermal conductivities of the materials, owing to variations in the internal moisture caused by different internal arrangements of the micropore structures and void size distributions, as shown in Figure 12. The heat transfer inside the specimens may have been affected by the non-uniform heat transfer path owing to the presence of connected and isolated air voids, as shown in Figure 17. The thermal conductivity of air is very low compared to that of the paste, and, as a poor conductor, it can reduce the overall thermal conductivity. Small air voids can limit heat flow by increasing the surface area for heat exchange. Therefore, different microstructures can exhibit different thermal performances. Additionally, owing to the different testing ages of the specimens, the drying ages also differed, resulting in varying moisture states for different micropore structures, which could be another factor affecting thermal conductivity. Moisture has a higher thermal conductivity than air, and it is expected that internal moisture (free water and physically bound water) may alter the rate of heat transfer in the specimens. After preparation, the PoroPCM specimens were kept in a controlled environment at 20±2.0 °C and a relative humidity (RH) of 60±2% for 28 and 35 d ages of Series 1 and 2 specimens respectively. Different drying times may cause variations in the internal moisture content of the porous specimens. To avoid the effect of internal moisture on the thermal performance of the PoroPCM, it is recommended that the specimens be dried prior to the experiment. In addition, to evaluate the thermal performance of PoroPCMs, the void ratio, internal structure of the void networks, and moisture equilibrium states should be considered.

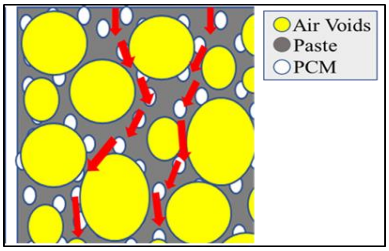

Fig. 17 Non-uniform heat transfer path due to air voids

4.4 Mechanical performance

Figure 18 shows the load–displacement curves of Specimens 1 and 2 and an image of Series 1–40 specimens after the compression test. In the figures, multiple load peaks are observed after the first peak load, and the loads are sustained even after large deformations, especially in higher air void cases, which may be due to the local collapse of the internal pore (or void) walls during the compression load. Deformation increased with porosity because the pore wall thickness decreased, and several local collapses occurred, which led to large deformations and caused the failure behavior to become ductile. Bötzow [27] reported failure mechanisms of highly porous cementitious materials. Under a compressive load, the interconnected pore walls of highly porous materials collapse, leading to failure of the pores (or voids), which considerably affects the failure mechanism of the specimens.

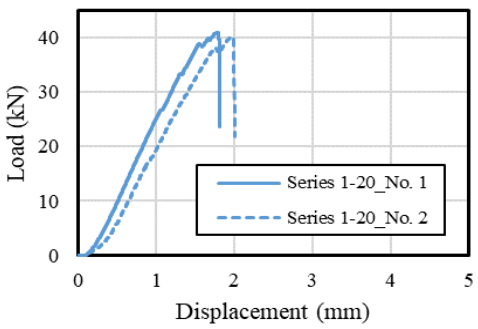

(a) Load–displacement curves for Series 1-20 specimens

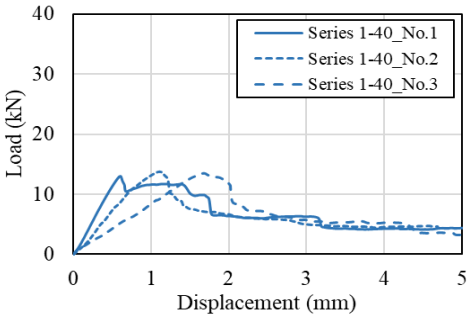

(b) Load–displacement curves for Series 1-40 specimens

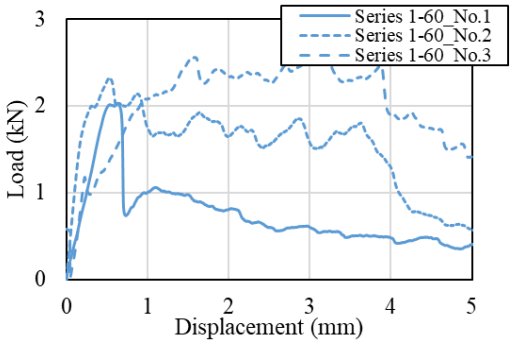

(c) Load–displacement curves for Series 1-60 specimens

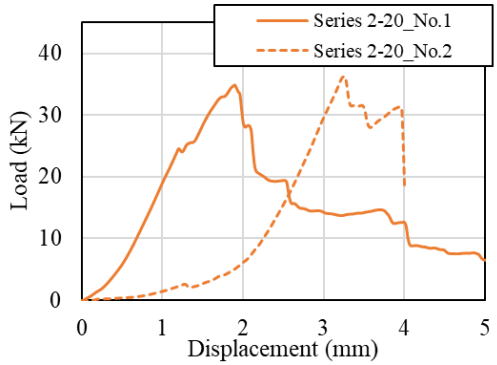

(d) Load–displacement curve for Series 2-20 specimens

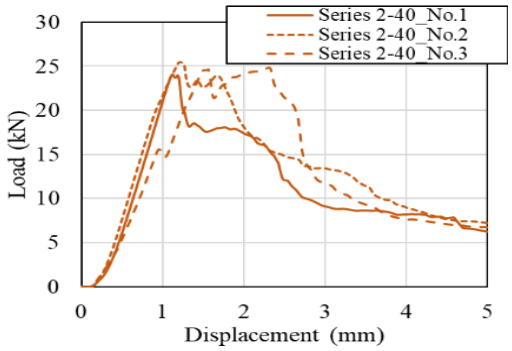

(e) Load–displacement curves for Series 2-40 specimens

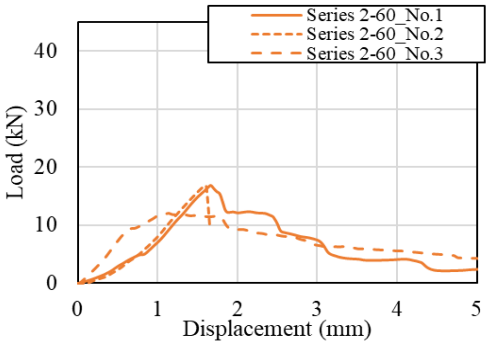

(f) Load–displacement curves for Series 2-60 specimens

(g) Photograph after compression test (Series 1-40 specimens)

Fig. 18 Ductile behavior of specimens during the compression test

Figure 19 shows the measured compressive strengths of the specimens. The compressive strength decreased significantly with increasing foam content. The compressive strength decreased by approximately 67% and 94% for Series 1 and 30% and 56% for Series 2 specimens with 40% and 60% foam PoroPCM, respectively, compared with 20% foam PoroPCM. The relationship between the compressive strength and the void ratio of the specimens is shown in Figure 20. The results show that the compressive strength is strongly correlated with the void ratio and is independent of the void size. This tendency differs from that of the thermal performance described in the previous section. As the porosity increases, the thickness of the pore walls decreases, thereby reducing the stiffness and strength. Thus, the volume of voids is an influential factor governing the strength of the PoroPCM.

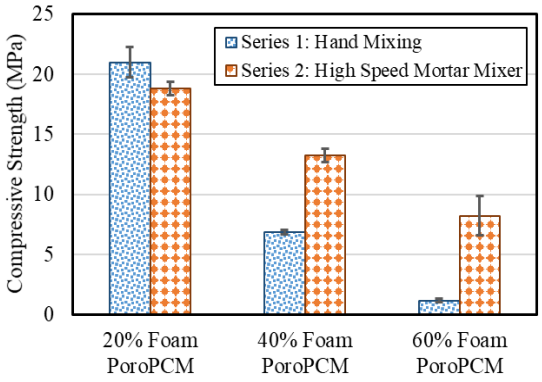

Fig. 19 Measured compressive strength

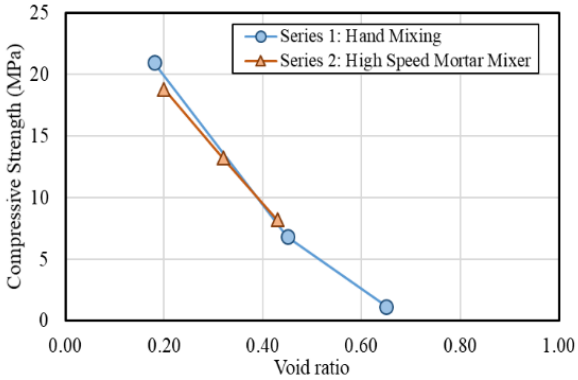

Fig. 20 Relationship between the compressive strength and void ratio

5 Conclusions

The focus of this study was to investigate the effect of microstructure on the thermal and mechanical behaviors of PoroPCM. An experimental study of PoroPCM was conducted with various porous structures to investigate the effect of the microstructure on its properties. Based on the experimental results, the following conclusions were drawn.

- The void structures and void ratios of the PoroPCM specimens were affected by the foam volume and mixing method. A gentle mixing procedure with low energy is preferred to maintain the high void ratio of PoroPCM.
- The void size in the PoroPCM specimens increased with void ratio, which may have been due to the overlapping and merging of air bubbles during mixing.
- The temperature-rise delay (shift of the peak temperature) observed owing to the phase transition of the MPCM and heat transfer may be influenced by the void ratio, microstructure, and internal moisture equilibrium state.
- The compressive strengths of the PoroPCM specimens were primarily influenced by the void ratios. The compressive strength decreased by approximately 67% and 94% for specimens with hand mixing and 30% and 56% for specimens with high-speed machine mixing with 40% and 60% foam PoroPCM, respectively, compared to the 20% foam PoroPCM case. With increasing void ratio, the thickness of the pore walls decreases, which leads to a reduction in strength. The failure behavior of the PoroPCM specimens under a compressive load was ductile failure with large deformation.

PoroPCMs have the potential to be viable solutions for thermal energy storage in buildings and cooling applications; however, further research and development are required to address the limitations and challenges associated with the material and its preparation process. These results are expected to enable engineers to extend the applications of PoroPCMs as insulating and thermal energy storage materials in the future. Although this study focused on the impact of porous microstructures on the thermal behavior of PoroPCM, further research is needed to understand the thermal properties (thermal conductivity, diffusivity, heat capacity, and latent heat) of the PoroPCM specimens, which will be addressed in future studies.

Acknowledgments

The authors acknowledge the grants and support from the EIG CONCERT-Japan Program offered by the Japan Science and Technology Agency. The authors are also thankful to MIKIRIKEN INDUSTRIAL for providing the phase-change materials used in this study and ASO FOAM CRETE CO., Ltd. for providing the aqueous foam.

Declaration of competing interest

The authors declare no competing interests relevant to the contents of this article.

Author contribution statement

All authors have given approval to the final version of the manuscript.

References

[1] P. K. S. Rathore and S. K. Shukla, “Enhanced thermophysical properties of organic PCM through shape stabilization for thermal energy storage in buildings: A state of the art review,” *Energy and Buildings*, vol. 236. Elsevier Ltd, Apr. 01, 2021, doi: 10.1016/j.enbuild.2021.110799.

[2] P. K. Singh Rathore, S. K. Shukla, and N. K. Gupta, “Potential of microencapsulated PCM for energy savings in buildings: A critical review,” *Sustainable Cities and Society*, vol. 53. Elsevier Ltd, Feb. 01, 2020, doi: 10.1016/j.scs.2019.101884.

[3] C. Mankel, A. Caggiano, N. Ukrainczyk, and E. Koenders, “Thermal energy storage characterization of cement-based systems containing microencapsulated-PCMs,” *Constr. Build. Mater.*, vol. 199, pp. 307–320, 2019, doi: 10.1016/j.conbuildmat.2018.11.195.

[4] J. Červenka, M. Herzfeldt, A. Caggiano, and E. Koenders, “Evaluation of Thermal and Mechanical Properties of Demonstration Wall Utilizing Phase Change Cementitious Materials,” in *Acta Polytechnica CTU Proceedings*, 2022, vol. 38, no. I, pp. 502–508, doi: 10.14311/APP.2022.38.0502.

[5] A. Bouguerra, A. Ledhem, F. De Barquin, R. M. Dheilly, and M. Quéneudec, “Effect of Microstructure on The Mechanical And Thermal Properties of Lightweight Concrete Prepared From Clay, Cement, And Wood Aggregates,” *Cem. Concr. Res.*, vol. 28, no. 8, pp. 1179–1190, 1998.

[6] V. V. Tyagi, S. C. Kaushik, S. K. Tyagi, and T. Akiyama, “Development of phase change materials based microencapsulated technology for buildings: A review,” *Renew. Sustain. Energy Rev.*, vol. 15, no. 2, pp. 1373–1391, 2011, doi: 10.1016/j.rser.2010.10.006.

[7] L. Chica and A. Alzate, “Cellular concrete review: New trends for application in construction,” *Constr. Build. Mater.*, vol. 200, pp. 637–647, 2019, doi: 10.1016/j.conbuildmat.2018.12.136.

[8] L. Hou, J. Li, Z. Lu, and Y. Niu, "Influence of foaming agent on cement and foam concrete," *Constr. Build. Mater.*, vol. 280, p. 122399, 2021, doi: 10.1016/j.conbuildmat.2021.122399.

[9] S. Wei, C. Yiqiang, Z. Yunsheng, and M. R. Jones, "Characterization and simulation of microstructure and thermal properties of foamed concrete," *Constr. Build. Mater.*, vol. 47, pp. 1278–1291, 2013, doi: 10.1016/j.conbuildmat.2013.06.027.

[10] D. Zhang, S. Ding, Y. Ma, and Q. Yang, "Preparation and Properties of Foam Concrete Incorporating Fly Ash," *Materials (Basel).*, vol. 15, no. 18, 2022, doi: 10.3390/ma15186287.

[11] R. Krishnamoorthy and J. A. Zujip, "Thermal Conductivity and Microstructure of Concrete Using Recycle Glass as a Fine Aggregate Replacement," *Eng. Mater. Sci.*, 2013.

[12] C. Lian, Y. Zhuge, and S. Beecham, "The relationship between porosity and strength for porous concrete," *Constr. Build. Mater.*, vol. 25, no. 11, pp. 4294–4298, 2011, doi: 10.1016/j.conbuildmat.2011.05.005.

[13] T. Nguyen, A. Ghazlan, A. Kashani, S. Bordas, and T. Ngo, "3D meso-scale modelling of foamed concrete based on X-ray Computed Tomography," *Constr. Build. Mater.*, vol. 188, pp. 583–598, Nov. 2018, doi: 10.1016/j.conbuildmat.2018.08.085.

[14] F. Batool and V. Bindiganavile, "Air-void size distribution of cement based foam and its effect on thermal conductivity," *Constr. Build. Mater.*, vol. 149, pp. 17–28, Sep. 2017, doi: 10.1016/j.conbuildmat.2017.05.114.

[15] S. Y. Chung, C. Lehmann, M. A. Elrahman, and D. Stephan, "Pore characteristics and their effects on the material properties of foamed concrete evaluated using micro-CT images and numerical approaches," *Appl. Sci.*, vol. 7, no. 6, 2017, doi: 10.3390/app7060550.

[16] M. S. Lebedev, M. I. Kozhukhova, and E. V. Voitovich, "Applicability of X-ray computed tomography for concrete cellular structure analysis," in *Journal of Physics: Conference Series*, Dec. 2021, vol. 2124, no. 1, doi: 10.1088/1742-6596/2124/1/012007.

[17] E. K. K. Nambiar and K. Ramamurthy, "Air-void characterisation of foam concrete," *Cem. Concr. Res.*, vol. 37, no. 2, pp. 221–230, 2007, doi: 10.1016/j.cemconres.2006.10.009.

[18] F. Batool, "Effect of Microstructure on Thermal Conductivity of Cement-Based Foam," 2015.

[19] F. Batool and V. Bindiganavile, "Air-void size distribution of cement based foam and its effect on thermal conductivity," *Constr. Build. Mater.*, vol. 149, pp. 17–28, 2017, doi: 10.1016/j.conbuildmat.2017.05.114.

[20] D. Snoeck, B. Priem, P. Dubruel, and N. De Belie, "Encapsulated Phase-Change Materials as additives in cementitious materials to promote thermal comfort in concrete constructions," *Mater. Struct. Constr.*, vol. 49, no. 1–2, pp. 225–239, 2016, doi: 10.1617/s11527-014-0490-5.

[21] M. Sam, A. Caggiano, L. Dubyey, J. L. Dauvergne, and E. Koenders, "Thermo-physical and mechanical investigation of cementitious composites enhanced with microencapsulated phase change materials for thermal energy storage," *Constr. Build. Mater.*, vol. 340, Jul. 2022, doi: 10.1016/j.conbuildmat.2022.127585.

[22] P. Jayalath, Amitha San Nicolas, Rackel Sofi, Massoud Shanks, Robert Ngo, Tuan Aye, Lu Mendis, "Properties of cementitious mortar and concrete containing micro-encapsulated phase change materials," *Constr. Build. Mater.*, vol. 120, pp. 408–417, 2016, doi: 10.1016/j.conbuildmat.2016.05.116.

[23] S. R. L. da Cunha and J. L. B. de Aguiar, "Phase change materials and energy efficiency of buildings: A review of knowledge," *J. Energy Storage*, vol. 27, no. November 2019, 2020, doi: 10.1016/j.est.2019.101083.

[24] L. Vásárhelyi, Z. Kónya, Kukovecz, and R. Vajtai, "Microcomputed tomography–based characterization of advanced materials: a review," *Mater. Today Adv.*, vol. 8, pp. 1–13, 2020, doi: 10.1016/j.mtadv.2020.100084.

[25] C. Halverson, "Characterization of geomaterials with X-ray computed tomography (X-ray CT)," *Master Thesis, Iowa State Univ.*, 2008.

[26] J. R. Gostick J, Khan ZA, Tranter TG, Kok MDR, Agnaou M, Sadeghi MA, "PoreSpy: A Python Toolkit for Quantitative Analysis of Porous Media Images," 2019.

[27] A. Gilka-Bötzow, P. Folino, A. Maier, E. A. B. Koenders, and A. Caggiano, "Triaxial failure behavior of highly porous cementitious foams used as heat insulation," *Processes*, vol. 9, no. 8, pp. 1–15, 2021, doi: 10.3390/pr9081373.

Md Suman Mia attained his bachelor's and master's degrees from the Dhaka University of Engineering & Technology (DUET), Gazipur, Bangladesh. He pursued Ph.D. at the Concrete Laboratory, Graduate School of Engineering, University of Tokyo, Japan. Md. Suman Mia currently serves as an assistant professor in the Department of Civil Engineering at DUET. His two research papers were published in DUET Journal and Advances in Materials Science and Engineering.